

Designing Perpetual Energy Harvesting Systems explained with RiverMote: A Wireless Sensor Network Platform for River Monitoring

Philipp Maria Glatz*

Leander Bernd Hörmann

Christian Steger

Reinhold Weiss

Institute for Technical Informatics, Graz University of Technology, Inffeldgasse 16/1, 8010 Graz, Austria

**Corresponding author*

Email: Philipp.Glatz@TUGraz.at, Glatz.Philipp@GMail.com

ABSTRACT: Wireless Sensor Network (WSN) motes are devices of small form factor. They are tailored to cost-effectiveness for monitoring and control applications. Different optimizations exist for the robust lifetime improvement of such devices, but the community still lacks a clear approach of how to achieve a robust system design that is of low cost and implements low-power optimizations. In particular, it is a demanding task to efficiently utilize energy harvesting system (EHS) technology for WSNs. However, that is the only way for implementing battery-free mote devices for achieving perpetual operation of WSNs. We demonstrate the design methodology that let us implement RiverMote. RiverMote is a case study for designing a low cost hardware system architecture combining low-power mote and a highly efficient EHS architecture. First, we provide a detailed explanation for how to deduce the prototype dimensioning parameters given the application requirements of an energy-autarkic river level monitoring system. Then we show how to select proper energy harvesting device (EHD) technologies and design all EHS stages for fitting the application-depending power state model of the integrated mote. Finally, we implement and evaluate tests of all stages for their energy efficiency as well as RiverMote's self-measurement accuracy which is crucial for robust perpetual designs.

1 INTRODUCTION AND MOTIVATION

Wireless sensor network (WSN) motes [1] are small networked embedded devices offering low-cost solutions to various applications. Though WSNs offer diverse functionality and a range of platforms, protocols and optimizations for dependability and powering issues [2], several lessons have been learned for how WSN deployments may fail partly or completely when it comes to real world deployments and issues with dynamic environments.

The Great Duck Island experience [3] is a prominent example for problems being experienced due to misconceptions of how dependability issues and power dissipation may interact. More recent deployments keep on experiencing different issues over and over again when it comes to mapping theory to deployments [4]. WSN deployments for environmental monitoring have to cope with changing environmental conditions. A well-known example discussing WSN deployment issues is given by [5].

The majority of optimization techniques for WSNs boil down to either (i) reducing the average power dissipation per end-user performance, (ii)

dealing with dependability issues, or (iii) to handle energy more efficiently from an electrical engineering point of view.

Using energy harvesting systems (EHSs) is the state of the art approach of providing more energy and longer lifetime or even energy neutral operation (ENO) until technical breakdown. When designing EHS-enhanced WSNs, different types of optimization (i)-(iii) need to be considered at the same time.

However, conditions for developing EHSs turn out to be more complex [6] than designing WSN motes alone. First, this is due to more complex hardware and software. Second, when it comes to ENO dependability issues, all possible scenarios and faults that may occur need to be taken into account. Especially the power profiles of energy harvesting devices (EHDs) and their effects are not precisely predictable. Therefore, protocols and policies are difficult to validate with simulation-based approaches. Furthermore, EHS and EHD selection and design are subject to trading hardware system cost against robustness and computational complexity when profiling and estimating EHD profiles and dealing with their effects. EHS design is concerned with introducing different kinds of thresholds for energy budgets, synchronization and back-off times while preserving end-user performance. The problem is that consider-

ing all these aspects results in EHS-enhanced WSNs being designed for ENO, but suffering efficiency loss due to dependability protocol overhead or energy safety bounds.

Although EHS technology is in the process of maturing and several important aspects have been considered and optimized, the authors of this article could not find design methodologies for robust and efficient EHS-enhanced WSN platforms. Here, we contribute with describing the design methodology of a highly efficient EHS and a robust low-power mote platform.

1.1 Contribution Claim

We state that there is a lack of self-contained design methodologies for EHS architectures for WSNs. Therefore, we present such a methodology combining the definition of application requirements, power estimation and power state models (PSMs), EHS design and EHD selection as well as designing energy storage requirements for achieving ENO. Tests will be run given worst case settings that are known to be challenging for existing EHS technology. Furthermore, the integration of accurate self-measurement as well as safety bounds and fallback mechanisms into RiverMote will be explained in detail. Hardware components have been selected such that the overall system cost (including water proof and UV resistant housing and all hardware) is similar to state of the art motes like TelosB [7] and Mica2 [8] platforms with a sensor-board attached.

RiverMote is a perpetual energy autarkic battery-free design and can be deployed with empty energy reservoirs. A robust design is established through using a dual DLC architecture with a balancing circuit. Efficient load matching is implemented with no need for maximum power point tracking (MPPT). It outperforms state of the art approaches in terms of input to output energy efficiency. Accurate characterization of efficiency plus accurate on-board measurement circuitry allows for intelligent behaviour. The approach is complete, extensible and easy to use.

2 RELATED WORK

Different EHSs have been developed so far with different issues and end-user performance in mind. For achieving an EHS design tailored to an application at hand, it is important to set up a proper PSM or to have a profiling tool of suitable accuracy available. Therefore, we present in-situ measurements and tools for characterization and simulation that are of similar accuracy as well. Finally, we will give a brief overview on EHD pattern prediction and ENO modelling.

2.1 EHS Enhanced WSNs

Different types of EHDs [9] can be used and different kind of EHS architectures can be implemented. Starting with HelioMote [10] different EHSs have made use of solar energy [11], [12], [13], [14]. It is the most convenient energy source for environmental monitoring applications [15]. While HelioMote uses batteries for its energy storage, there are prominent examples of EHS architectures using DLCs like Everlast [16] and AmbiMax [17] and even specific approaches exploring different DLC storage architectures [18].

Designing an EHS consists of two main tasks. First, the load's energy demands are modelled with a mote PSM with regard to application requirements. Second, possible EHS designs have to be evaluated using an expressive EHS efficiency model (EEM). Accurately measured PSM and EEM parameters are discussed in [19]. Furthermore, offline analysis results (usually by simulation) need to be validated by runtime measurements.

Different techniques impact the EEM usually trading energy efficiency for measurement accuracy or hardware cost and robustness. As an example, the simple trade-off of whether a shunt-based measurement system should be implemented in the supply path or at ground side is discussed for an embedded energy monitor [20]. A number of decisions of different complexity need to be made when designing an EHS and tuning an EEM.

When designing an EHS, a substantial trade-off is whether MPPT should be implemented or not. It may improve system efficiency, but it leads to more complex hardware or software and will increase platform cost. Everlast and AmbiMax both implement MPPT, where [16] uses CPU intervention and [17] implements a hardware mechanism. MPPT might be used if EHS efficiency is increased at reasonable hardware cost leading to more end-user performance while achieving ENO. MPPT need not be used if load-matching can be implemented efficiently by other means.

2.2 Runtime Power Dissipation Measurement

Different direct and indirect debugging and profiling techniques exist. While passive software based approaches exist – consider passive network inspection in [21] – we will concentrate on more direct and hardware-related approaches for power profiling.

PowerBench [22], SPOT [20] and the energy measurement board in [23] are well-known examples for sandwich-on in-situ measurement boards. These systems are meant to be used for WSN motes that are of similar form factor as RiverMote is intended to be. SPOT is designed with subject to meeting accuracy requirements similar to what RiverMote current measurements need to accomplish.

They define a power dissipation spectrum that needs to be measured with a given accuracy. However, what is missing is a clear definition of the maximum error that is still acceptable. The sum of the integral of weighted power states' errors could be upper bounded and tested for worst case examples. That is what will be done for RiverMote. A given power state measurement's error impact on the final application and its Duty Cycle (DC) will be considered.

A neat approach for deducing the worst case error as presented in [19] helps in identifying and in optimizing single sources of error. With integrating the information into suitable simulation environments, [24] allows to model the maximum error that may occur when measuring energy from the EHDs and supplying it to the mote. Combining this information with the maximum variation of EHDs' patterns that can be expected and PSM error bounds allows introducing overall thresholds and single stages' safety bounds for not violating the ENO condition.

2.3 ENO and Energy Thresholds

The most common type of modelling ENO for EHS-enhanced WSNs is ρ/σ -modelling as introduced and discussed for this type of technology in [25] and [26]. However, an evaluation on hardware in [6] shows sensitivity of such systems to variable EHD patterns. This may quickly lead to an unstable network given the fact that hardware is being designed to be cost efficient combined with changing environments and inherently unstable embedded devices' wireless communication. Summing up the power loss at different stages of the EHS - and adding errors of EEM and PSM runtime measurements where necessary - as well as introducing suitable thresholds for worst case solar irradiation given long-term meteorological data of the deployment region has not been done so far.

From a conceptual point of view the approach presented by HydroWatch [27] is similar to what is presented here. We neatly describe the methodology behind designing and testing RiverMote. The RiverMote target application will be similar to [28], but measurements will be performed with in-situ techniques placed directly into the water with components that are lightweight in terms of hardware cost and power consumption. This allows designing a more efficient architecture still being capable of ENO at less cost compared to allowing power dissipation of up to 3W in [28].

3 RIVERMOTE DESIGN

The design phase starts with determining the application requirements and outlining possible sensor technologies. Then, the PSD and EEM requirements

can be deduced and the system can be designed according to their characteristics.

3.1 Application Requirements and Sensor Choices

RiverMote shall be capable of real-time river level monitoring. The required accuracy of the water level measurements depends on the specific application. Three possibilities for measuring the level are considered important: using a pressure transducer, GPS leveling and ultrasonic transceivers. All three are outlined briefly. The latter two are integrated and tested with RiverMote and hardware interfaces are implemented for the first. Firstly, with a pressure transducer one can get very accurate results, but accurate waterproof sensors are quite expensive. Furthermore, the sensor needs to be placed on ground of the river which may be problematic. Secondly, using a GPS receiver offers a solution where cost of the GPS device and complexity of the correction algorithm can be traded for accuracy improvements. It also has the advantage that it can be placed inside the mote's housing and can be used for a number of other application scenarios as well. Thirdly, ultrasonic transceivers can be attached to the mote's housing and are easy to use. Though they deliver inherently noisy measurements, the sensor readings can be post processed which can give accurate measurements with cheap hardware. A related project in [29] shows how embedded ranging technologies can be optimized with expressive simulations so that results hold for deployments as well.

Finally, one has to define the sampling frequency that is needed to fulfil the given task. Therefore we first define the radio to have a range in the order of several hundred meter. So a large scale deployment is still possible without the need for adding GSM or 3G support which will in turn save costs. Furthermore, the water level measurement principles demand for a fixed base station outside the water for differential measurements like changing barometric pressure anyway. This base station - which is more or less the same RiverMote hardware, but is supplied via USB and not from a solar cell - allows reading out the measurement results from a RiverMote network in range. For being able to capture river level effects with motes deployed 1km apart from each other a maximum sampling period of 5-15min allows to accurately track river flood waves. Given these application characteristics, we design and dimension different stages of the mote and its EHS according to the resulting energy needs. We add energy thresholds where appropriate to achieve a robust design. In addition, we implement hardware fallback mechanisms that stabilizes a RiverMote's energy budget in case erroneous application behaviour or software or network policies drain the energy reservoir.

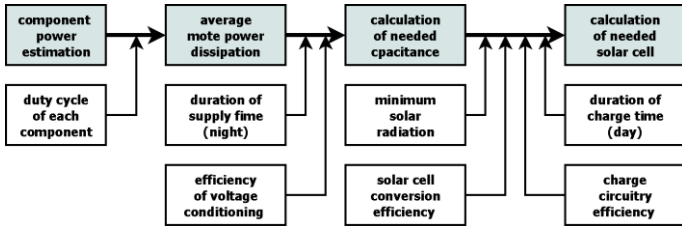


Figure 1. Calculation methodology of the DLC capacitance and the size of the solar cell.

3.2 Power Supply

The battery-less mote must harvest sufficient energy from the environment. It operates outside on the surface of a river and is exposed to the daylight. Therefore, a solar EHD is used to supply RiverMote. A little generator using the flow of the river has been considered too, but the problem of a mechanical system is that the generator has to be placed outside the housing and therefore is prone to errors. RiverMote is designed maintenance-free with solar cells. The needed size and consequently the output power depend on the power consumption of the mote including leakage and errors that occur when profiling power dissipation online. While explaining the power estimation process later we start with outlining the storage structure first.

3.3 Energy Storage

There are mainly two possibilities to store the electrical energy. First, the energy can be stored in a rechargeable battery and second it can be stored in a DLC. Batteries have much more capacity compared to the DLCs, but the disadvantages of batteries are their much more limited lifetime and temperature dependencies.

Neglecting temperature dependencies of embedded systems may lead to hard-to-debug errors when the system is deployed. Therefore, we evaluate RiverMote during a Winter in Austria where hardware temperature is measured to vary for approximately 50 degrees each day.

A DLC has typically 500.000 charge-discharge cycles and a nominal lifetime of 10 years. In contrast to that, a NiMH battery has lifetime of only 500 charge-discharge cycles before experiencing a capacity loss of down to 80% [10]. Energy harvested during day must be stored in the energy storage device for continuous monitoring during night as well. This is only a short time and can be bridged with a DLC which is not impacted by the high number of recharge cycles. The needed capacity depends on the power consumption of the overall hardware architecture. Furthermore, a hysteresis is implemented in hardware that will only switch on the mote if enough energy can be offered for full hardware and network initialization. This results in a design, such that even completely wrong software configurations (activat-

Table 1. The MSP430F1611 MCU has been selected for TinyOS compatibility reasons. The MRF24J40MB has been selected as the ZigBee radio due to its range and versatile capabilities including printed antenna. The pressure transducer and the ultrasonic sensor will be switched off completely. Therefore, they have a power consumption of zero during sleep state. An activation interval of 15min is assumed here. A GPS Fastrax UP300 has been chosen due to its internal backup capabilities for its initially found configuration.

Component	t_a [s]	P_a [mW]	P_{sl} [mW]	P_{avg} [mW]
MCU	30	5.0	0.1	0.60
Send	2	429.0	0.0	0.95
Receive	28	82.5	0.0	2.57
RxTx Sleep	30	0.0	0.1	0.10
GPS	30	120.0	0.1	4.10
Pressure	1	250.0	0.0	0.28
Ultrasonic	1	10.0	0.0	0.01
Other HW	30	30.0	0.1	1.10
Total P_{tot}				9.70

ing all components all the time) do not drain RiverMote below its lower energy threshold before a network join and software reconfiguration is possible.

The design is such that the time of being fully drained is lower bounded by the application DC period and the maximum time for component initialization. For RiverMote, this bound clearly depends on the time for downloading an initial GPS configuration and storing it persistently after a full reset. Designing RiverMote this way will also lead to a blackout sustainability of several weeks despite the fact that the design is battery-free. Although not explained in further detail, we mention here that the back-off energy reservoir easily fits into the energy reservoir of the storage architecture range that will be deduced.

Back to dimensioning the storage architecture, the energy stored in capacitors can be calculated with:

$$E = \frac{C \cdot U^2}{2}, E = \frac{C \cdot (U_C \cdot n)^2}{2 \cdot n}, E = \frac{C \cdot n \cdot U_C^2}{2} \quad (1)$$

The voltage U has a quadratic effect and DLCs usually have a very low nominal voltage. Therefore, two DLCs have been connected in series. The resulting capacity is only half the capacity of a single capacitor, but the nominal voltage doubles and this has a higher effect on the overall storable energy.

Unfortunately, the gain in storable energy does not come for free. Additional hardware is needed to balance the DLCs and keep them from exceeding their operating voltage. So, each additional DLC can be traded for power lost and cost of a further balancing circuitry between each of the DLCs. It can be seen that the number of capacitors connected in series directly impacts the energy budget calculation and RiverMote's system cost.

3.4 Power Estimation and Energy Storage Device

Table 1 shows a list of RiverMote's components and their expected power dissipation for implementing the application scenario. Their values make up a coarse grain PSM that is used for the calculations shown in Figure 1. The components are active for t_a seconds during each period time T which leads to a DC and average power dissipation of 9.7 mW.

$$D = \frac{t_a}{T}, P_{avg} = D \cdot P_a + (1 - D) \cdot P_{sl} \quad (2)$$

For further calculation a higher value of 12mW will be used. The maximum current that the EHS must be capable of supplying can be calculated from summing up all power dissipation over supply voltage.

$$I_{max, full} = \frac{P_{max, full}}{U_{sup}} = \frac{854mW}{3.3V} = 258.8mA \quad (3)$$

Now, one can design the energy storage structure according to the longest night during midwinter. Austria is south of the 49th latitude. The longest night lasts for about 15 h and 40 min. Here, we assume 16 h:

$$E_{blackout} = P_{tot} \cdot t_{night} = 12mW \cdot 16h = 691.2J \quad (4)$$

The energy stored in the capacitor must be converted to supply the mote. For lossy conversion an efficiency of 80% is assumed. Now, the energy that must be stored in the capacitor can be calculated:

$$E_{needed} = \frac{E_{blackout}}{\eta_{convert}} = \frac{691.2J}{0.8} = 864J \quad (5)$$

As mentioned before, it is better to connect capacitors in series to increase the storable energy. In this project, two capacitors will be connected in series. A typical nominal voltage of a DLC is 2.5V. Therefore, the resulting nominal voltage is $U_n = 5V$. Using a converter operating from 1.8V capacity gives:

$$C_{real} = \frac{2 \cdot E_{needed}}{U_{start}^2 - U_{stop}^2} = \frac{2 \cdot 864J}{(5V)^2 - (1.8V)^2} = 79.41F \quad (6)$$

In this project, two Boostcap® DLCs with a nominal voltage of 2.5V and a capacity of 310F are used. Connected in series they provide a usable energy of

$$E_{usable} = \frac{C \cdot (U_{start}^2 - U_{stop}^2)}{2} = 1686.4J \quad (7)$$

and a maximum power consumption of the mote of

$$P_{max} = \frac{E_{usable} \cdot \eta_{convert}}{t} = \frac{1686.4J \cdot 0.8}{16h} = 23.42mW \quad (8)$$

The maximum DLC leakage current is 0.45mA.

$$P_{leakage} \leq I_{leakage} \cdot U_n = 0.45mA \cdot 5V = 2.25mW \quad (9)$$

The highest tractable mote power dissipation is.

$$P_{tot, max} \geq P_{max} - P_{leakage} = 23.42 - 2.25 = 21.17mW \quad (10)$$

In theory, RiverMote can easily be supplied by the structure. Detailed practical evaluation will be given.

3.5 Solar Cell Calculation

Finally, the power needed and consequently the size of the solar cell will be calculated. Storing energy from the EHD is not lossless. With 80% input efficiency the total energy needed per day is 1036.8J.

$$E_{24h} = P_{tot} \cdot (t_{day} + t_{night}) = 1036.8J \quad (11)$$

Adding leakage, input and conversion efficiencies

$$E_{24h, leakage} = P_{leakage} \cdot (t_{day} + t_{night}) = 194.4J \quad (12)$$

$$E_{24h, solar} = \frac{E_{24h}}{\eta_{charge} \cdot \eta_{convert}} + \frac{E_{24h, leakage}}{\eta_{charge}} = 1863J \quad (13)$$

the total solar power can be calculated with:

$$P_{solar} = \frac{E_{24h, solar}}{t_{day}} = \frac{1863J}{8h} = 64.69mW \quad (14)$$

This power must be provided by the solar cell also during days with bad weather conditions. A monthly-averaged horizontal daily extra-terrestrial irradiation of $P_{D, avg} = 2120W/m^2$ at a latitude of 50° in December is mentioned in [30]. The converting coefficient of solar light into electrical power is about 10%. Therefore, the needed solar radiation and solar cell size can be calculated with:

$$P_{radiation} = \frac{P_{solar}}{\eta_{day}} = \frac{64.69mW}{0.1} = 646.9mW \quad (15)$$

$$A_{cell, sun} = \frac{P_{radiation}}{P_{D, avg}} = \frac{646.9mW}{212mW/cm^2} = 3.05cm^2 \quad (16)$$

A worst-case scenario must be considered, where the DLC can only store the energy needed for one night of continuous operation. The minimum solar irradiation (power density) at a very cloudy and rainy day is about $P_{D, min} = 3mW/cm^2$ [31]. This is equal to a radiation of $30W/m^2$. The value is coherent with the diagrams on page 37 in [30]. Now, the needed area of the solar cell can finally be calculated as follows.

$$A_{cell} = \frac{P_{radiation}}{P_{D, min}} = \frac{649.9mW}{3mW/cm^2} = 215.6cm^2 \quad (17)$$

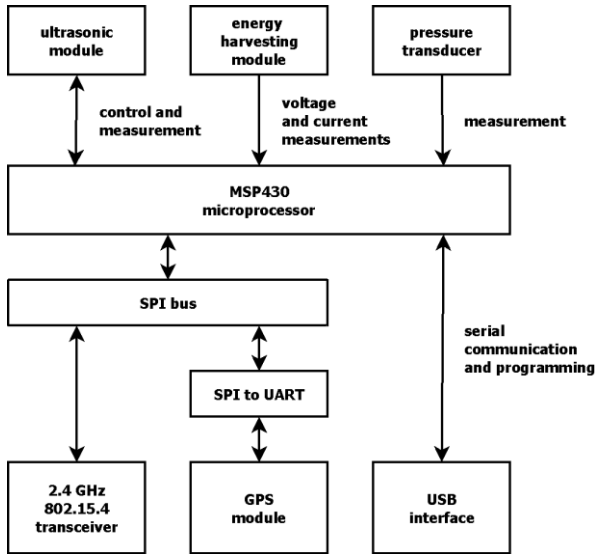


Figure 2. RiverMote hardware modules and interfaces.

The resulting size of the solar cell is suitable to be integrated into the housing. Therefore, a compact and robust system can be built. If it would not match needs, model parameters would have to be tuned.

4 SYSTEM IMPLEMENTATION AND SETUP

The system setup consists of mote and EHS implementation.

4.1 Mote Hardware Design

Figure 2 depicts RiverMote's components built around the MSP430F1611 low-power microcontroller from Texas Instruments®. The GPS receiver needs an extra serial interface. An SPI-to-UART adapter is used. It receives data from the SPI and transmits it to the GPS receiver and vice versa. No direct connection to the microcontroller is needed. The 2.4GHz 802.15.4 transceiver module is connected to the SPI as well for fast and easy communication. The ultrasonic module and the EHS module are directly connected. Ultrasonic control lines are directly operated by the MSP430 whereas the EHS can operate completely control-free so that software errors cannot alter system robustness. Current and voltage measurements can be done directly by the MSP430. Programming RiverMote via a bootstrap loader and runtime communication for debugging and configuration from a PC-connected base station RiverMote can be done directly via USB.

4.2 Energy Harvesting System Design

Figure 3 shows a block diagram of the EHS part. The solar cell transforms the solar energy into electrical energy. It is a voltage limited current source. A short is no problem for a solar cell. The electrical power will be converted into heat in the solar cell

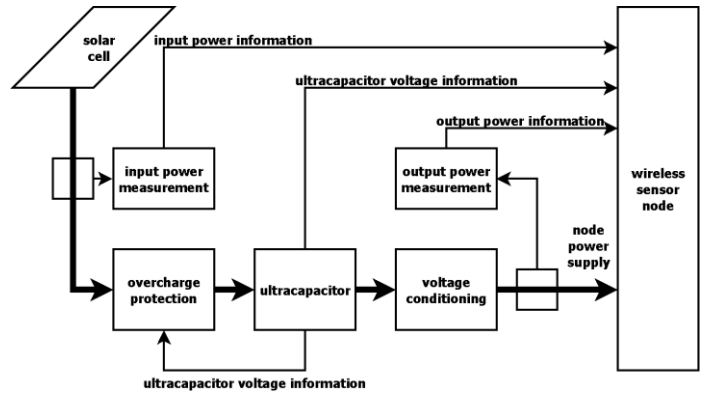


Figure 3. RiverMote control and power design.

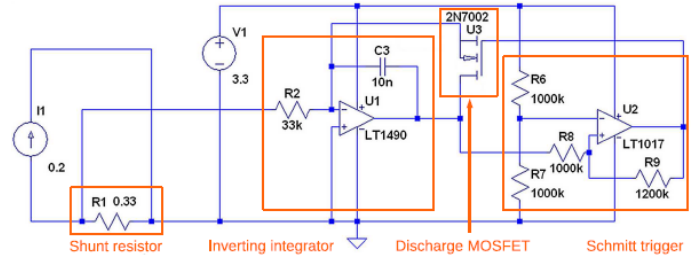


Figure 4. Circuit diagram of the current counter with its inverting integrator and Schmitt trigger[3] as main parts.

and the connecting leads. As can be seen in Figure 2, no voltage conditioning is done between the solar cell and the DLCs. This can only be done if the solar cell is selected appropriately and connected in line with the DLCs. Section 5 will show results on the EHS's input efficiency that results from this design. High efficiency is achieved without any need for costly additional hardware or control for load matching mechanisms. The voltage of the solar cell at nominal power output should be a little bit higher than the nominal voltage of the DLCs. This is because some losses and a lower output voltage of the solar cell at dark light conditions must be considered. The solar cell ASI3Oo05/162/192FAMod from Schott Solar has been selected. An overcharge protection guarantees a maximum voltage at the DLCs. Voltage conditioning is used to generate a stable output voltage at 3.3V, because most of the components are supplied with this voltage. The voltage at the DLCs changes during operation and must be stabilized with a buck-boost converter. The stored energy and the input and output power must be measured, because the system needs to know the current energy state. Then the system is able to select a proper DC to ensure continuous operation. Figure 4 shows the circuit diagram. The voltage drop over shunt resistor R1 is input to the integrator. This voltage is accumulated by the integrator until a certain threshold is reached. This threshold is given by the upper threshold of the Schmitt trigger. Next, the integrating capacitor C3 is discharged via MOSFET U3 down to the lower threshold. Then, a pulse used as current counter is generated and the process starts again. Figure 5 shows a RiverMote prototype implementation without a solar cell or housing.

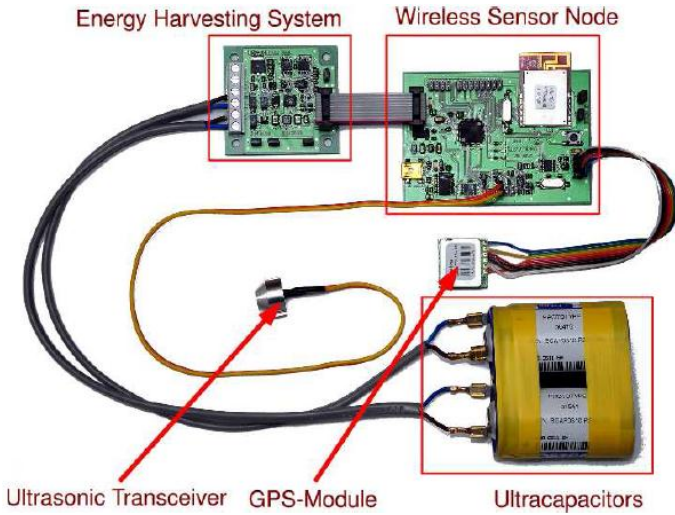


Figure 5. Photograph of a RiverMote prototype.

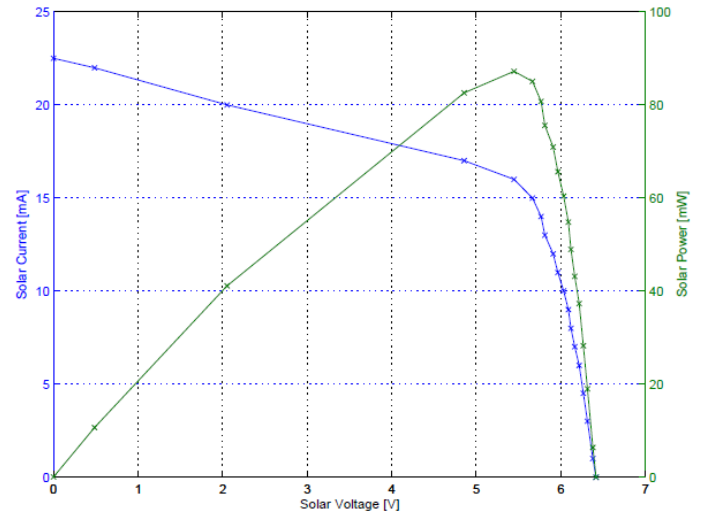


Figure 7. Profiling solar cell characteristics.

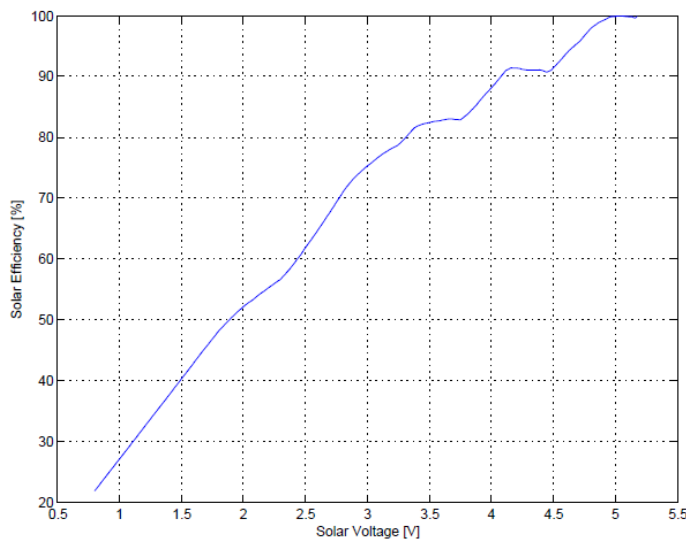


Figure 6. Solar efficiency depending on input clamp voltage.

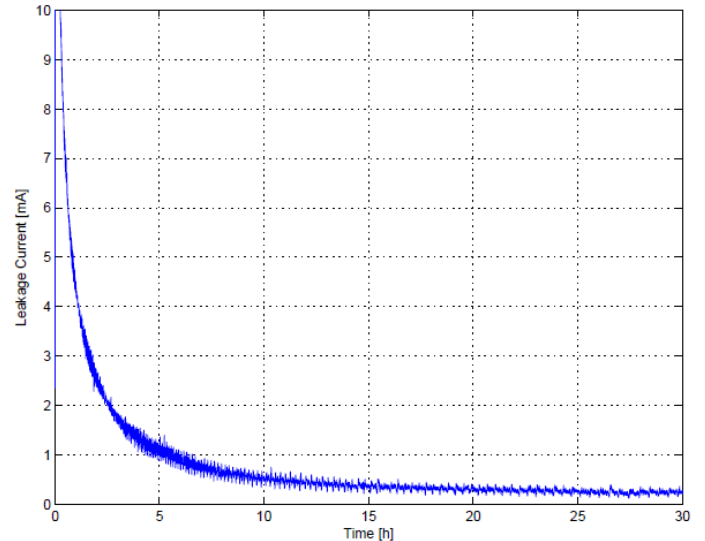


Figure 8. The DLC leakage current is settling down.

5 PLATFORM EVALUATION

Evaluation includes input efficiency of the solar cells, effects of DLC loading and its leakage, overall EEM, measurement circuitry evaluation, long-term measurements, sensor, radio and cost issues.

5.1 Solar Cell Evaluation

Figure 6 shows V-I characteristics of the solar cell for bad light conditions on a cloudy December day with its maximum power point at 5.5V which will be lower for better conditions. This perfectly suits the design of RiverMote. Figure 7 shows the solar efficiency during the charging process for solar efficiency for the maximum power point being 100%:

$$\eta_{solar} = \frac{P_{solar}}{\max(P_{solar})} \cdot 100\% \quad (18)$$

It can be seen that the solar efficiency is better than 80% if the voltage of the DLCs is higher than 3V. In this case, the solar voltage is about $U_{solar} = 3.4V$, because of the forward voltage of the Schottky diode. Therefore, the voltage of the DLCs should be kept as high as possible.

5.2 Capacitor Leakage

DLC leakage current has been measured after charging the DLC and disconnecting the power supply.

$$I_{leak} = \frac{C \cdot \Delta U_{cap}}{\Delta t} = C \cdot \left(U_{cap, n+1} - U_{cap, n} \right) \cdot rate \quad (19)$$

The average leakage current during the whole measurement was 0.487mA. This is slightly above the

Table 2. Key results of EHS efficiency measurements.

Description	Value
Maximum stored energy in the capacitor	1233.10J
Minimum stored energy in the capacitor	998.52J
Dynamic energy of the capacitor	234.57J
Maximum capacitor voltage	3.99V
Minimum capacitor voltage	3.59V
Dynamic voltage of the capacitor	0.40V
Duration of a high-power period	18.02min
Duration of a low-power period	55.41min
Duty-Cycle	0.33
Average input current	21.57mA
Average input power	88.07mW
Average output power	73.24mW
Total Efficiency of the EHS	83.16%

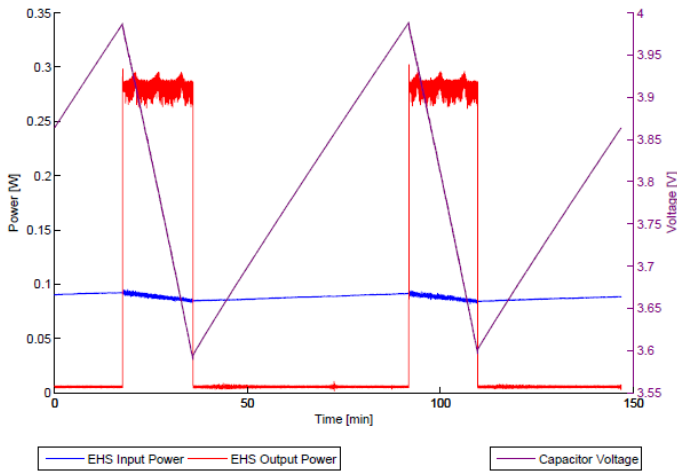


Figure 9. EHS efficiency measurements.

expected leakage current according to the data sheet which is 0.45mA [32] with an initial peak of more than 10mA. However, the significant value of the leakage current is the average leakage current of the first 16 hours after disconnecting the power supply. This time span must be bridged with the DLC. The average leakage current during this interval was 1.398mA. Conditions are relaxed again, because it must be considered that the DLC was disconnected immediately after reaching the maximum voltage of 2.5V. A second measurement was done. The maximum voltage was kept constant for one day. After this time, the DLC was disconnected and the leakage current was measured. Figure 8 shows that there is no initial peak any more. The average leakage current during the first 16 hours is 0.121mA. So, we can get down below a third of the value of the data sheet.

5.3 Capacitor Balancing

The balancing circuit is needed for not overcharging the DLCs due to unbalanced charging with only one combined overcharge protection for both. The balancing current at a difference of 0.2V is 10mA. The maximum charge current of the DLCs can be calculated with the results of the previous measurement.

The tolerance is $\pm 20\%$ ($d = 0.2$) for the capacitors. The worst-case scenario and total capacity is:

$$C_1 = C \cdot (1 - d), C_2 = C \cdot (1 + d), C_{tot} = C \frac{1 - d^2}{2} \quad (20)$$

The total charge is equal to that of the single DLCs:

$$Q_{tot} = Q_{uc1} = Q_{uc2} = Q_{full, ch} \cdot C \cdot \frac{1 - d^2}{2} = 744As \quad (21)$$

The smaller capacitor's voltage after charging is:

$$U_{uc1} = \frac{Q_{uc1}}{C_{DLC,1}} = U_{full, ch} \cdot \frac{1 + d}{2} = 5V \cdot \frac{1.2}{2} = 3V \quad (22)$$

The difference to the surge voltage of the DLC is:

$$\Delta U_{max} = U_{uc1} - U_{max} = 0.3V \Rightarrow \Delta Q = \Delta U_{max} \cdot C_1 = 74.4As \quad (23)$$

Now, the minimum charging time can be calculated:

$$t_{ch} = \frac{\Delta Q}{I_{bal, 0.4V}} = \frac{\Delta Q}{I_{bal, meas, 0.2V} \cdot 2} = \frac{74.4As}{20mA} = 3720s \quad (24)$$

Thus the maximum charging current is:

$$I_{ch} = \frac{\Delta Q}{t_{ch}} = \frac{74.4As}{3720s} = 200mA \quad (25)$$

The maximum charging current constraint is greatly relaxed, because the discharge threshold is set to be 1.8V. The selected solar cells can be used.

5.4 EHS Efficiency Evaluation

The measurement setup presented in [19] is used for the measurements. The input power and the output power can be calculated with:

$$P_{input} = U_2 \frac{U_{R_2}}{R_2}, P_{output} = U_1 \frac{U_{R_1}}{R_1} \quad (26)$$

EHS efficiency and the stored energy are as follows.

$$\eta_{EHS} = P_{output} / P_{input}, E_{stored} = \frac{1}{2} \cdot C \cdot U^2 \quad (27)$$

Figure 9 shows two charge-discharge cycles of the DLCs. The key results of this measurement are listed in Table 2. The input current during the whole measurement was $I_{in} = 21.57mA$. The small variation of the input power is caused by the changing voltage of the DLCs. The resulting efficiency of 83.16% is better than expected. The efficiency consists of the efficiency of input circuit and the efficiency of the output circuit. Both have been assumed to be 80%. The resulting efficiency of the EHS would have been 64%. Therefore, the real circuit is much better than expected and no additional MPPT hardware needs to be implemented. RiverMote's efficiency outperforms other EHS approaches.

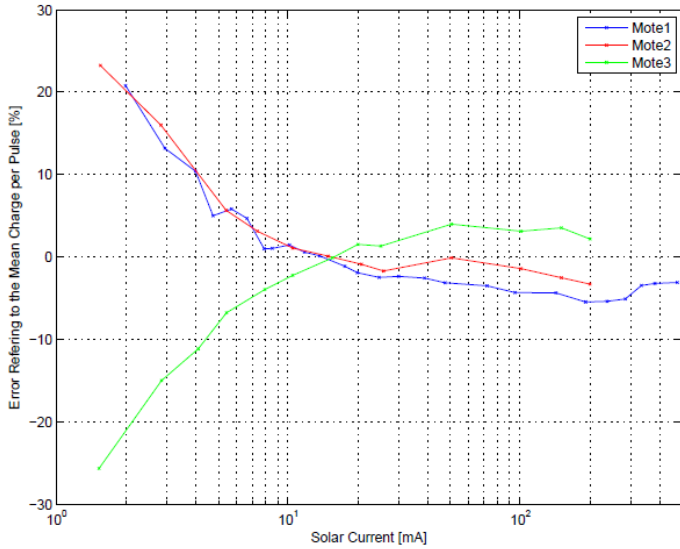


Figure 10. Relative error of the solar current counter.

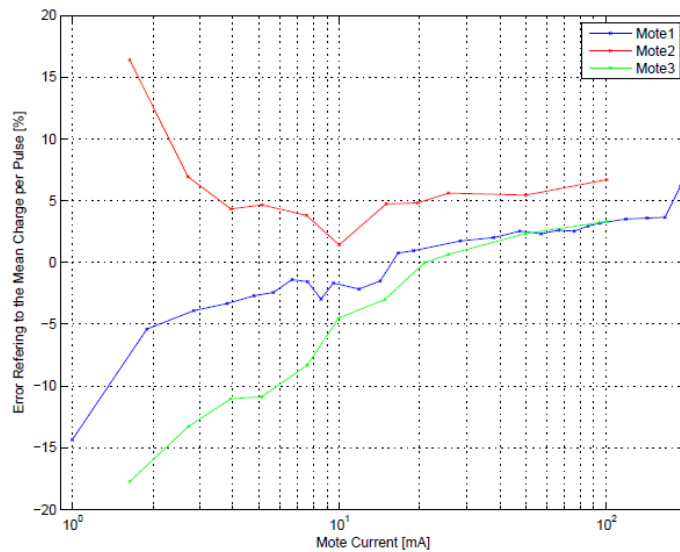


Figure 11. Relative error of the mote current counter.

Already the output efficiency alone of the EHS in [6] has been characterized in [19] to vary for up to 50%.

5.5 Current Measurement Error Evaluation

Figure 10 shows that the error can increase to 20% at low solar currents. However, it works properly at high enough solar currents and the error at lower values does not violate ENO conditions due to thresholds introduced in the system. The solar current is higher than 10mA during daytime even at bad weather conditions. Therefore, the error of the solar current counter is better than 10% during daytime. The error of the mote current measurement depending on the mote current is shown in Figure 11. It can be seen that the error is up to 20% at low mote currents. However, similar conditions apply as for the mote current measurement. Due to the fact that the current of the mote is about 1.5mA in LPM 3, the impact of an error of the current measurement of

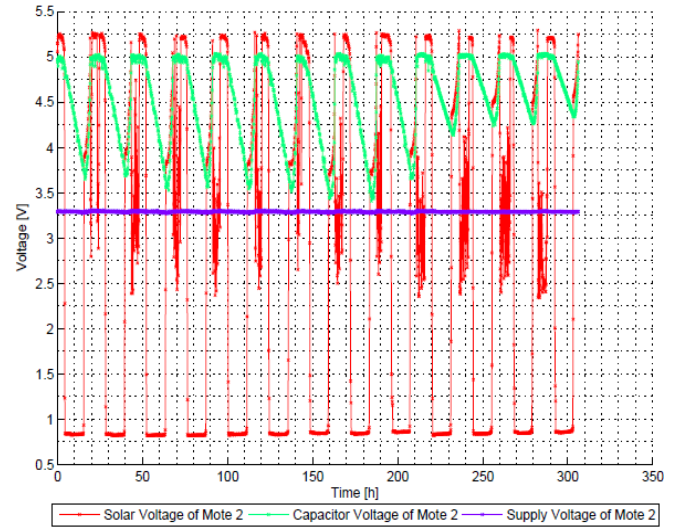


Figure 12. Voltage measurements of RiverMote 2.

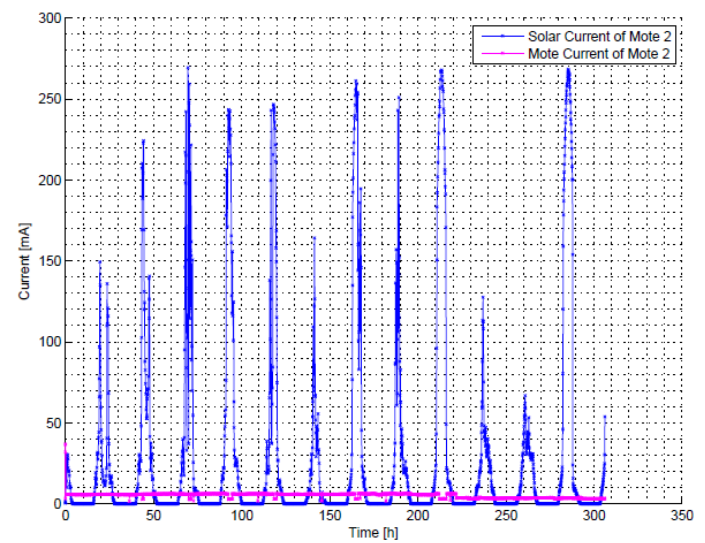


Figure 13. Current measurements of RiverMote 2.

20% is still below the DLC leakage as defined in its data sheet.

5.6 Long-Term Evaluation

Here we present the results of the long-term measurements using RiverMotes 2 and 3. Both motes are initially configured to send their data every 10min. Mote 2 is placed under a clear-transparent cover. Mote 3 is mounted in a water-proof housing with a greyish transparent cover. Both motes measure their energy state and the temperature of the environment. Figure 12 shows the measured voltages of mote 2. Mote 3 has shown similar results. The RiverMotes operate continuously without manually recharging the DLCs even during days of bad weather. Figure 13 shows the current of mote 2 – again mote 3 has shown similar results. The traces of the input and output power have been similar to the traces of the solar and mote current and are left out for brevity. Tests show that the temperature in the housing varies up to 50°C per day as can be seen in Figure 14.

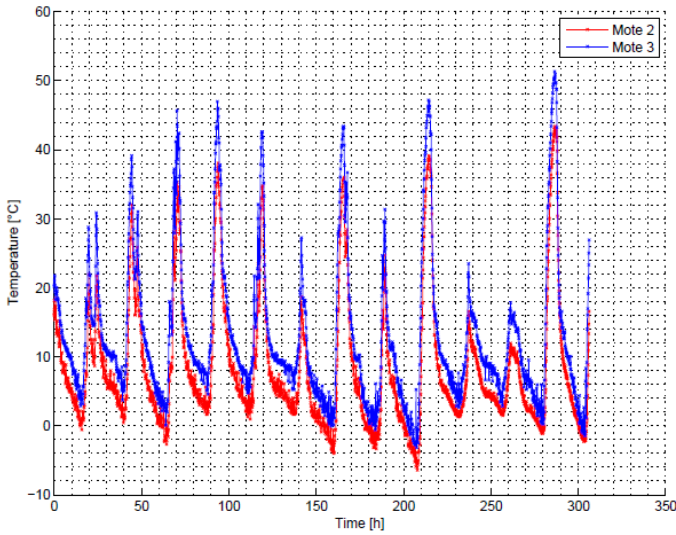


Figure 14. Temperatures measured at RiverMotes 2 and 3.

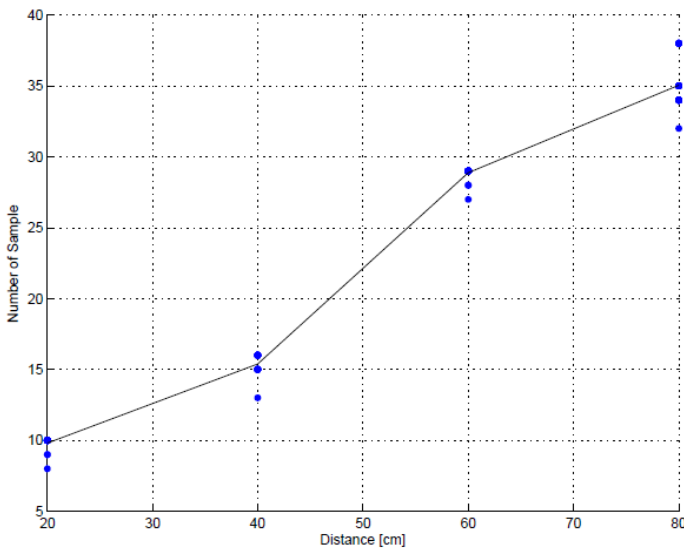


Figure 15. Ultrasonic distance measurements.

5.7 Sensor Accuracy

The ultrasonic transceiver and the GPS have been profiled for their accuracy. As expected, the GPS - without further post processing or applying differential GPS correction - gives only coarse results. The results for initialization after reset and movement along the shore of Schwarzlsee near Graz is shown in Figure 16. Mote 3 is carried down the shore and back again. The basics of the measurement principle are working, but further post processing will be needed for accurate measurements. Another option for achieving accurate results is using the ultrasonic transceiver which can be quite accurate as shown in Figure 15.

5.8 Communication Range Evaluation

The range measurements are taken at Schwarzlsee near Graz as well. The receiver is placed on the dashboard of a car that moves at 35 km/h. Figure 17 shows that the system is working correctly even for large distances. It can be seen that most of the packets are received successfully. So, the radio can effi-

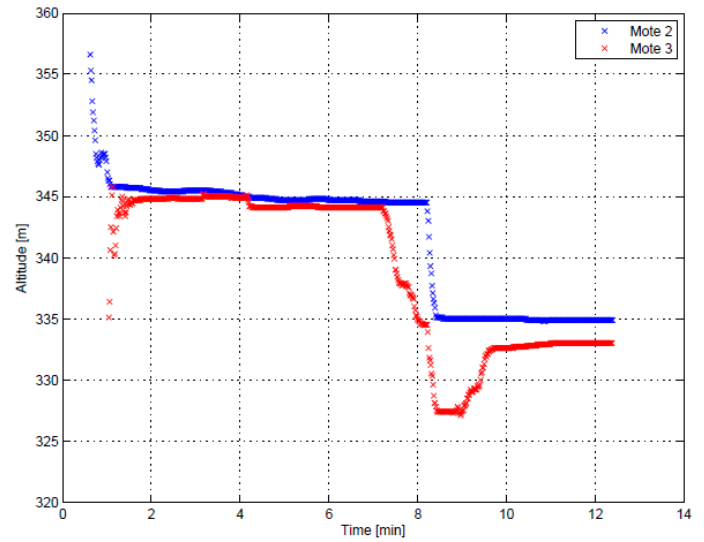


Figure 16. GPS leveling measurements.

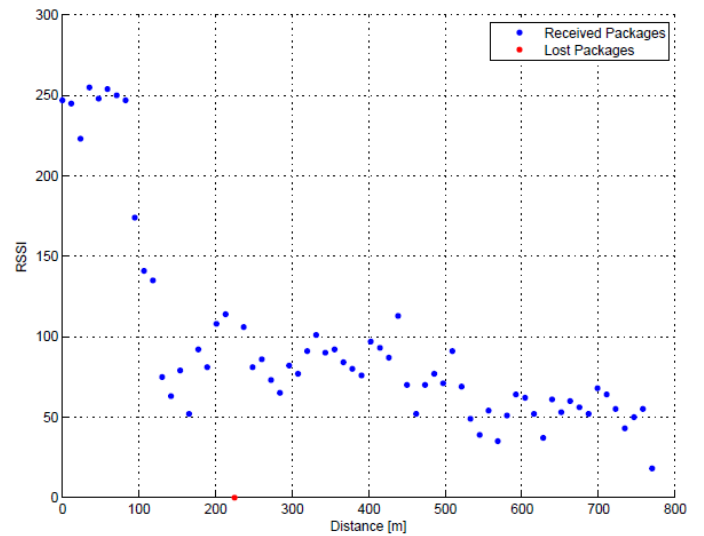


Figure 17. RSSI value over different distances.

ciently span large distances along river deployments. For an even more robust deployment we suggest to put 2 RiverMotes per km.

6 CONCLUSION AND FUTURE WORK

RiverMote – an EHS-enhanced WSN platform – is characterized along with a neat description of its design process. This includes setting up the application requirements, examining environmental conditions, EHD selection, EHS design, explicit and implicit measurement setups, component selection and mote design as well as testing and evaluation.

The design is battery-free. Solar cells are used for harvesting and DLCs are used for storing the energy. The setup can be reconfigured at runtime. This allows running the system as testbed as well. Long-term measurements' energy balance and power dissipation profiles are shown. The whole design process is performed in a way such that it leads to an energy autarkic platform and allows ENO. Dynamic reconfiguration allows adapting the end-user per-

formance and the energy drain. Erroneous conditions for draining the energy reservoir (e.g. with over-sampling the GPS) are tested. In case such software errors occur there are cheap hardware mechanisms that allow fully restarting and initializing a RiverMote and let it join the network again in a robust way. Additional hardware for protection, balancing, conversion and matching is analysed and implemented where appropriate. The highly efficient design is achieved with hardware of reasonably low cost. It is similar to state of the art motes without EHS. It offers different types of bus systems and connectors that allow easily attaching new sensor hardware, programming the system, and connecting a RiverMote that is working as a base station to a PC. A GPS receiver along with GPS leveling measurements and ultrasonic transducers have been integrated and profiled with the system.

Future directions are to add support for design decisions that are made when designing RiverMote or similar EHS-enhanced WSN platform to the TOSPIE2 environment [24]. Considering their design trade-offs and effects in its tools may contribute to the modelling and simulation environment. It could automatically be adapted to future EHS design descriptions and their PSMs and EEMs and be used for design space exploration when designing novel energy harvestings architectures.

7 REFERENCES

- [1] I. F. Akyildiz, W. Su, Y. Sankarasubramaniam, and E. Cayirci. Wireless sensor networks: a survey. *Comput. Netw.*, 2002.
- [2] J. Yick, B. Mukherjee, and D. Ghosal. Wireless sensor network survey. *Comput. Netw.*, 52(12), 2008.
- [3] A. Mainwaring, D. Culler, J. Polastre, R. Szewczyk, and J. Anderson. Wireless sensor networks for habitat monitoring. In *WSNA'02*, 2002.
- [4] J. Beutel and M. R. K. Römer, M. Woehrl. Deployment techniques for wireless sensor networks. *Sensor Networks: Where Theory Meets Practice*, 2009.
- [5] K. Langendoen, A. Baggio, and O. Visser. Murphy loves potatoes: Experiences from a pilot sensor network deployment in precision agriculture. *IPDPS'06*, 2006.
- [6] P. M. Glatz, P. Meyer, A. Janek, T. Trathnigg, C. Steger, and R. Weiss. A measurement platform for energy harvesting and software characterization in WSNs. In *Wireless Days 08*, 2008.
- [7] J. Polastre, R. Szewczyk, and D. Culler. Telos: enabling ultra-low power wireless research. In *IPSN'05*, 2005.
- [8] J. Hill and D. Culler. A wireless embedded sensor architecture for system-level optimization, 2001.
- [9] S. Chalasani and J. M. Conrad. A survey of energy harvesting sources for embedded systems. *IEEE Southeast Conference*, 2008.
- [10] V. Raghunathan, A. Kansal, J. Hsu, J. Friedman, and M. Srivastava. Design considerations for solar energy harvesting wireless embedded systems. In *IPSN'05*, 2005.
- [11] J. Jeong, X. Jiang, and D. Culler. Design and analysis of micro-solar power systems for wireless sensor networks. In *INSS'08*, 2008.
- [12] D. Brunelli, L. Benini, C. Moser, and L. Thiele. An efficient solar energy harvester for wireless sensor nodes. In *DATE'08*, 2008.
- [13] P. Stanley-Marbell and D. Marculescu. An 0.9 x 1.2", low power, energy-harvesting system with custom multi-channel communication interface. In *DATE '07*, 2007.
- [14] P. Corke, P. Valencia, P. Sikka, T. Wark, and L. Overs. Long-duration solar-powered wireless sensor networks. In *EmNets'07*, 2007.
- [15] C. Park, J. Liu, and P. H. Chou. Eco: an ultra-compact low-power wireless sensor node for real-time motion monitoring. In *IPSN'05*, 2005.
- [16] F. Simjee and P. H. Chou. Everlast: long-life, supercapacitor-operated wireless sensor node. In *ISLPED'06*, 2006.
- [17] C. Park and P. H. Chou. Ambimax: Autonomous energy harvesting platform for multi-supply wireless sensor nodes. *SECON'06*, 1, 2006.
- [18] A. Janek, C. Trummer, C. Steger, R. Weiss, J. Preishuber-Pfluegl, and M. Pistauer. Simulation based verification of energy storage architectures for higher class tags supported by energy harvesting devices. *Microprocess. Microsyst.*, 32(5-6), 2008.
- [19] P. M. Glatz, L. B. Hörmann, C. Steger, and R. Weiss. A system for accurate characterization of wireless sensor networks with power states and energy harvesting system efficiency. In *PerSeNS'10*, 2010.
- [20] X. Jiang, P. Dutta, D. Culler, and I. Stoica. Micro power meter for energy monitoring of wireless sensor networks at scale. In *IPSN'07*, 2007.
- [21] K. Römer and J. Ma. Pda: Passive distributed assertions for sensor networks. In *IPSN'09*, 2009.
- [22] I. Haratcherev, G. Halkes, T. Parker, O. Visser, and K. Langendoen. PowerBench: A Scalable Testbed Infrastructure for Benchmarking Power Consumption. In *IWSNE'08*, 2008.
- [23] T. Trathnigg and R. Weiss. Towards runtime support for energy awareness in wireless sensor networks. In *Notere'07*, pages 49–54, 2007.
- [24] P. M. Glatz, C. Steger, and R. Weiss. Poster abstract: Tospie2: Tiny operating system plug-in for energy estimation. In *IPSN'10*, 2010.
- [25] A. Kansal, J. Hsu, S. Zahedi, and M. B. Srivastava. Power management in energy harvesting sensor networks. *ACM Trans. Embed. Comput. Syst.*, 2007.
- [26] N. Jaggi, K. Kar, and A. Krishnamurthy. Near-optimal activation policies in rechargeable sensor networks under spatial correlations. *ACM Trans. Sen. Netw.*, 4(3), 2008.
- [27] J. Taneja, J. Jeong, and D. Culler. Design, modeling, and capacity planning for micro-solar power sensor networks. In *IPSN'08*, 2008.
- [28] D. Hughes, G. Blair, G. Coulson, P. Greenwood, B. Porter, P. Smith, and K. Beven. An adaptable wsnbased flood monitoring system. 2008.
- [29] P. M. Glatz, C. Steger, R. Weiss. Design, simulation and measurement of an accurate wireless sensor network localization system. In *PM2HW2N'10*, 2010.
- [30] T. Muneer. *Solar Radiation and Daylight Models*. Elsevier Butterworth-Heinemann, 2004.
- [31] SchottSolar. Asi oem outdoor solar modules.
- [32] MaxwellTechnologies. Datasheet bcap0310.